

# Pressure-induced structural evaluation and insulator-metal transition in the mixed spinel ferrite $\text{Zn}_{0.2}\text{Mg}_{0.8}\text{Fe}_2\text{O}_4$

S. Rahman,<sup>1,2</sup> Sudeshna Samanta,<sup>2</sup> D. Errandonea,<sup>3</sup> Shuai Yan,<sup>4</sup> Ke Yang,<sup>4</sup> Junling Lu,<sup>1,\*</sup> and Lin Wang<sup>2,†</sup><sup>1</sup>*Department of Chemical Physics, University of Science and Technology of China, Hefei, China*<sup>2</sup>*Center for High Pressure Science and Technology Advanced Research, Shanghai 201203, China*<sup>3</sup>*Departamento de Física Aplicada-Instituto Universitario de Ciencia de los Materiales de la Universidad de Valencia (ICMUV), MALTA Consolider Team, Universidad de Valencia, Edificio de Investigación, C/Dr. Moliner 50, Burjassot, 46100 Valencia, Spain*<sup>4</sup>*Shanghai Synchrotron Radiation Facility (SSRF), Shanghai Institute of Applied Physics, Chinese Academy of Science, Shanghai 201800, China*

(Received 17 October 2016; published 9 January 2017)

The effect of pressure on the electronic properties and crystal structure in a mixed spinel ferrite  $\text{Zn}_{0.2}\text{Mg}_{0.8}\text{Fe}_2\text{O}_4$  was studied for the first time up to 48 GPa at room temperature using x-ray diffraction, Raman spectroscopy, and electrical transport measurements. The sample was cubic (spinel-type  $Fd\bar{3}m$ ) at ambient pressure and underwent a pressure-induced structural transition to an orthorhombic phase ( $\text{CaTi}_2\text{O}_4$  – type  $Bbmm$ ) at 21 GPa. This structural transformation corresponded to a first-order phase transition that involved 7.5% molar volume shrinkage. The onset of the Mott insulator-metal transition (IMT) around 20 GPa was due to a spin crossover mechanism that led to the  $\text{Fe}^{3+}$  magnetic moment collapse. All the Raman modes disappeared at high pressures, which supported metallization. Analysis of structural and electrical transport measurements showed a simultaneous volume collapse and sharp IMT within a narrow pressure range. The orthorhombic high-pressure phase was found to have a higher conductivity than the cubic phase. The pressure dependence of the conductivity supported the metallic behavior of the high-pressure phase.

DOI: [10.1103/PhysRevB.95.024107](https://doi.org/10.1103/PhysRevB.95.024107)

## I. INTRODUCTION

Spinel ferrites containing iron oxides are important magnetic compounds and have attracted significant attention due to their unique magnetic properties such as high Curie temperature [1,2], high coercivity [2], large Kerr effect [2,3], and Faraday rotations [2,4]. Spinel ferrites are represented as  $AB_2X_4$  (where  $B = \text{Fe}$  for spinel ferrites) with two different coordination polyhedra for metal atoms (cations), which are located at the tetrahedral [ $A$ ] and octahedral [ $B$ ] sites in a [ $A$ ]:[ $B$ ] mole ratio of 1:2, while anions are generally oxygen atoms (oxospinel). The  $A\text{Fe}_2\text{O}_4$  compounds usually crystallize in cubic (isometric) symmetry space group  $Fd\bar{3}m$ . Categorically, spinels are normal and inverse on the basis of cation distribution, such as  $[A]^{tet}[\text{Fe}_2]^{oct}\text{O}_4$  (e.g.,  $\text{ZnFe}_2\text{O}_4$ ) [5,6] and  $[\text{Fe}]^{tet}[A\text{Fe}]^{oct}\text{O}_4$  (e.g.,  $\text{MgFe}_2\text{O}_4$ ) [7,8], respectively. Temperature ( $T$ ) and high pressure (HP) lead to disorder at tetrahedral and octahedral sites and tuning of the Neel temperature of magnetic spinels [2,9,10]. Different polymorphs can be induced under compression. In their diverse polymorphs, many interesting properties have been found, including insulator-metal transitions (IMTs), superconductivity, and colossal magnetoresistance due to the critical balance between crystal lattice distances and electronic degrees of freedom [11].

The crystal structure, electronic structure, and thermodynamic properties of spinel ferrites can be tuned externally by perturbations such as temperature and pressure [9]. From a geophysics perspective, seismic discontinuity in the Earth's mantle can be identified by the decomposition of magne-

siowüstite ( $\text{MgFe}_2\text{O}_4$ ) [12] and franklinite ( $\text{ZnFe}_2\text{O}_4$ ) [9,13] found in rocks. Hence, investigations on the HP behaviors of  $\text{ZnFe}_2\text{O}_4$  [9] and  $\text{MgFe}_2\text{O}_4$  [9,14] have important implications for understanding the dynamics of Earth's lower mantle. Results showed that both  $\text{ZnFe}_2\text{O}_4$  and  $\text{MgFe}_2\text{O}_4$  have highly dense orthorhombic  $\text{CaMn}_2\text{O}_4$ -type structures [15,16], which were found after a phase transition at 33 and 25 GPa, respectively. Recently, intermediate compounds with cosubstitution of metal divalent cations ( $A^a$  and  $A^b$ ), known as mixed ferrites formulated as  $[A^a]_{1-\delta}[\text{Fe}_\delta]^{tet}[A^b]_{\delta}[\text{Fe}_{2-\delta}]^{oct}\text{O}_4$ , such as  $\text{Zn}_x\text{Mg}_{1-x}\text{Fe}_2\text{O}_4$ , have gained interest [17–19]. However, their physical properties have been much less explored under HP. In previous studies, it was suggested that replacement of ion with a larger size of cation in the spinel may facilitate the transition into higher co-ordination structures at relatively lower pressures. Therefore,  $\text{Zn}_{0.2}\text{Mg}_{0.8}\text{Fe}_2\text{O}_4$  is considered to be a potential candidate for examining the pressure-induced phase transformation.

Since polymorphism often occurs at HPs, merely HP x-ray diffraction (XRD) cannot give sufficient information about physical properties of the postspinel phase [20,21], such as magnetism and conductivity. Unfortunately, there is a complete lack of HP data on electrical resistivity measurements apart from the parent compound  $\text{Fe}_3\text{O}_4$ , where a nonmetallic HP phase was achieved [22] that was associated with a structural transition, which involved a ferromagnetic-paramagnetic transition. The highest conductivity in  $\text{Fe}_3\text{O}_4$  with  $\rho \sim 4.3 \times 10^3 \Omega \text{ cm}$  was explained by polaronic hopping, where normal and inverse spinels  $\text{ZnFe}_2\text{O}_4$  and  $\text{MgFe}_2\text{O}_4$  have conductivities  $\rho \sim 10^2 \Omega \text{ cm}$  and  $\rho \sim 10^7 \Omega \text{ cm}$ , respectively [2,23–25] due to the incomplete substitution of  $\text{Fe}^{2+}$  with  $\text{Zn}^{2+}/\text{Mg}^{2+}$ , leading to normal configuration. It was experimentally demonstrated [26] that intermediate compounds can have maximum conductivity when metal ions and  $\text{Fe}^{3+}$  ions at the tetrahedral

\*Corresponding author: junling@ustc.edu.cn

†Corresponding author: wanglin@hpstar.ac.cn

sites are almost equal. Supported by this understanding, we found a high-resistive cubic phase with  $\rho \sim 2\text{--}7 \times 10^4 \Omega \text{ cm}$ , which transformed into a HP low-resistive (bad metallic) orthorhombic phase with  $\rho \sim 0.7 \times 10^3 \Omega \text{ cm}$  occurring at 33 GPa.

In this paper, we investigated a HP-induced phase transition in  $\text{Zn}_{(x)}\text{Mg}_{(1-x)}\text{Fe}_2\text{O}_4$  ( $x = 0.2$ ) by synchrotron XRD, where existing Mössbauer spectroscopy measurements confirmed that its local magnetic ordering remained intact when  $x \leq 0.4$  [17,18]. The Mössbauer spectra can be resolved into two subspectra, corresponding to the distribution of Fe ions in the tetrahedral sites and other Fe ions in the octahedral sites. After successful structure refinements, we observed a pressure-induced phase transition at about  $\sim 22$  GPa, having the HP phase an orthorhombic postspinel structure, which has not been reported so far. Earlier reports on Mössbauer spectroscopy suggest that the HP orthorhombic phase is not magnetically ordered [27,28]. Studies on pressure-induced phase transitions in cubic spinels [29,30] are still not fully understood, and there are disagreements regarding postspinel structures [29,30]. Hence, understanding the dynamics of mixed ferrites such as  $\text{Zn}_{0.2}\text{Mg}_{0.8}\text{Fe}_2\text{O}_4$  with XRD, Raman spectroscopy, and electrical measurements under HP is the main focus of our paper.

## II. EXPERIMENTAL

The spinel sample  $\text{Zn}_{0.2}\text{Mg}_{0.8}\text{Fe}_2\text{O}_4$  was synthesized by the conventional ceramic method [31]. All reagents  $\text{ZnO}$ ,  $\text{MgO}$ , and  $\text{Fe}_2\text{O}_3$  were mixed with purified water according to their weight ratio and dried in a furnace at  $150^\circ\text{C}$  for 4 h. The dried mixture was ball-milled for six hours to obtain fine powders and slowly cooled to room temperature (RT). The extracted powder was further ground and crushed for 30 minutes before second round sintering for 5 h at  $1100^\circ\text{C}$ . We used the final powder sample for all our experiments.

We performed RT, HP XRD measurements for  $\text{Zn}_{0.2}\text{Mg}_{0.8}\text{Fe}_2\text{O}_4$  at the Shanghai Synchrotron Radiation Facility (SSRF, BL15U1 beamline), China, with x-ray wavelength  $0.6199 \text{ \AA}$ . All HP experiments were carried out in a symmetric diamond anvil cell (DAC) with a steel gasket and silicone oil as our pressure-transmitting medium. Sample pressures were determined using the calibrated ruby pressure standard of Mao *et al.* [32]. The XRD patterns were collected using a Mar165 CCD detector. The resulting ring-type diffraction patterns were integrated using the Fit2D software. Rietveld refinement analyses were carried out using the FULLPROF software [33]. From the refinements, we have identified crystal structures and determined the pressure dependence of the lattice parameters.

Raman spectroscopy experiments were completed using an inVia Renishaw Raman spectrometer system with a laser wavelength  $512 \text{ nm}$  and a grating of  $2400 \text{ g/cm}$ . The range of our interest was  $100\text{--}850 \text{ cm}^{-1}$ . Similar to XRD, we used silicon oil as pressure-transmitting media during measurements under HP. The wavenumbers of the Raman peaks were determined with an accuracy of  $1 \text{ cm}^{-1}$ .

The HP electrical resistivity measurements were performed using the standard four-probe technique in a DAC up to 35 GPa. The gasket was insulated with a mixture of epoxy and cubic

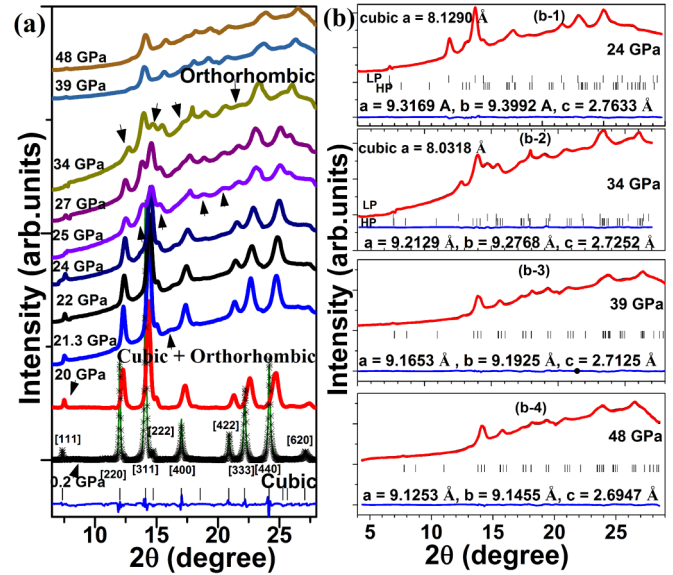


FIG. 1. (a) Angle-dispersive XRD patterns for  $\text{Zn}_{0.2}\text{Mg}_{0.8}\text{Fe}_2\text{O}_4$  at different pressures at RT. The  $\uparrow$  depicts the appearance of new HP phase peaks, and  $\downarrow$  indicates the disappearance of LP phase peaks. (b) Rietveld refinements for the new HP phases at 24, 34, 39, and 48 GPa, respectively.

boron nitride. Four platinum leads were arranged to contact the sample in the chamber. No pressure medium was used for resistivity measurement. The resistance was determined by the van der Pauw method [34].

## III. RESULTS

### A. Pressure-induced structural changes from XRD

Figure 1(a) represents the XRD spectra at different pressures. The indexes ( $hkl$ ) of the Bragg peaks are marked for the ambient-pressure phase of  $\text{Zn}_{0.2}\text{Mg}_{0.8}\text{Fe}_2\text{O}_4$ . This phase has a cubic structure that belongs to space group  $Fd\bar{3}m$  [35]. We found no considerable change in the diffraction peaks below 20 GPa, except that the peaks gradually shifted towards high angles due to the decrease of the unit-cell parameter. New diffraction peaks appeared at 21.3 GPa and grew in intensity with further increasing pressure. They became pronounced at 25 GPa. Rietveld profile fittings showed that the best agreement between the observed and calculated patterns was achieved by considering multiphase refinements that assumed an orthorhombic  $\text{CaTi}_2\text{O}_4$ -type structure and cubic spinel structure simultaneously, as shown in Fig. 1(b) (b-1 and b-2). Therein, the new diffraction peaks at  $13.7^\circ$ ,  $15.3^\circ$ ,  $18.8^\circ$ , and  $20.4^\circ$  were assigned to an orthorhombic structure. Our observation is consistent with the literature, which reports that cubic spinels often transform to an orthorhombic phase under HP [35,36]. The estimated pressure for the onset of the phase transition is  $P \sim 22$  GPa. The most dominant factor for this phase change is the disorder and rearrangements of octahedral ( $B$  Sites) and tetrahedral ( $A$  Sites) [9,36].

Numerous studies show that most cubic spinels transform to an orthorhombic phase upon pressure increase [35,36]. We concluded from these Rietveld refinements that the cubic spinel and HP phase coexisted for  $21 \text{ GPa} < P < 34 \text{ GPa}$ ,

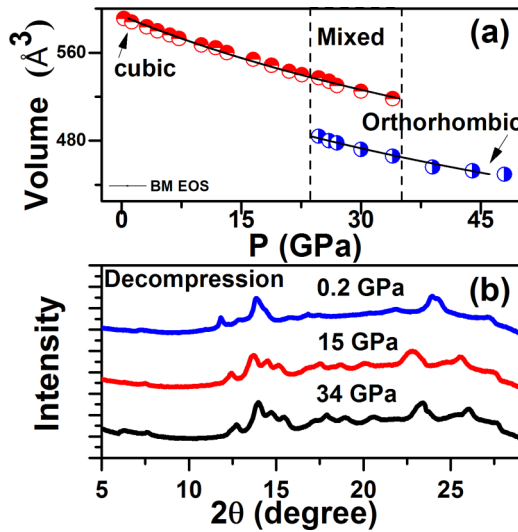


FIG. 2. (a) Unit cell volume as a function of pressure in the cubic and orthorhombic phases. (b) The XRD spectra of  $\text{Zn}_{0.2}\text{Mg}_{0.8}\text{Fe}_2\text{O}_4$  in the decompression run.

as shown in Fig. 1(b) (b-1 and b-2). At 24 GPa, we obtained  $a = 9.3169 \text{ \AA}$ ,  $b = 9.3992 \text{ \AA}$ , and  $c = 2.7633 \text{ \AA}$  for the orthorhombic structure and  $a = 8.1290 \text{ \AA}$  for the cubic structure. Above 25 GPa, the orthorhombic phase started to dominate, peaks became much broader, and many of them split due to anisotropic compression of the orthorhombic structure.

At 34 GPa, the Rietveld refinements gave lattice constant parameters  $a = 8.013 \text{ \AA}$  for cubic and  $a = 9.2129 \text{ \AA}$ ,  $b = 9.2768 \text{ \AA}$ , and  $c = 2.7252 \text{ \AA}$  for the orthorhombic structure with multiphase profile-matching parameters  $R_p = 1.46\%$ ,  $R_{wp} = 1.93\%$ , and  $\chi^2 = 1.72$ . According to the intensity ratio, 71.3% of the sample was in the HP phase, and 28.7% of the sample was in the low-pressure (LP) phase. Above 39 GPa, a single orthorhombic phase was observed, as shown in Fig. 1(b) (b-3 and b-4). Rietveld analysis provided the structure of the single phase  $\text{CaTi}_2\text{O}_4$ -type with space group  $Bbmm$ ,  $Z = 4$ , with lattice parameters  $a = 9.1653 \text{ \AA}$ ,  $b = 9.1925 \text{ \AA}$ , and  $c = 2.7125 \text{ \AA}$  at 39 GPa. Certainly, we cannot exclude other orthorhombic structures such as  $\text{CaMn}_2\text{O}_4$  (space group  $Pbcm$ ) and  $\text{CaFe}_2\text{O}_4$  (space group  $Pnma$ ) as they closely resemble the assigned structure. The HP phase is denser than the spinel phase. In addition, cations change their coordination from octahedral and tetrahedral to octahedral to dodecahedral [37]. This pressure-induced cubic-orthorhombic phase transition involves an increase of the material density by approximately 7.5%, as a result of volume collapse. This volume discontinuity can be seen in Fig. 2(a) [15].

The pressure-volume data was fitted with the third-order Birch-Murnaghan equation of state (BM-EOS) [35]:

$$P = \frac{3}{2}K_0[(V_0/V)^{7/3} - (V_0/V)^{5/3}][1 - (3/4)(4 - K'_0) \times [(V_0/V)^{2/3} - 1]], \quad (1)$$

where  $K_0$  is the bulk modulus,  $K'_0$  is the first derivative of the bulk modulus, and  $V_0$  is the unit cell volume. Calculations provided  $V_0 = 596.7(8) \text{ \AA}^3$ ,  $K_0 = 194(5)$ , and  $K'_0 = 3.8(4)$  for the LP phase and  $V_0 = 267.8(8) \text{ \AA}^3$ ,  $K_0 = 193(5)$ , and

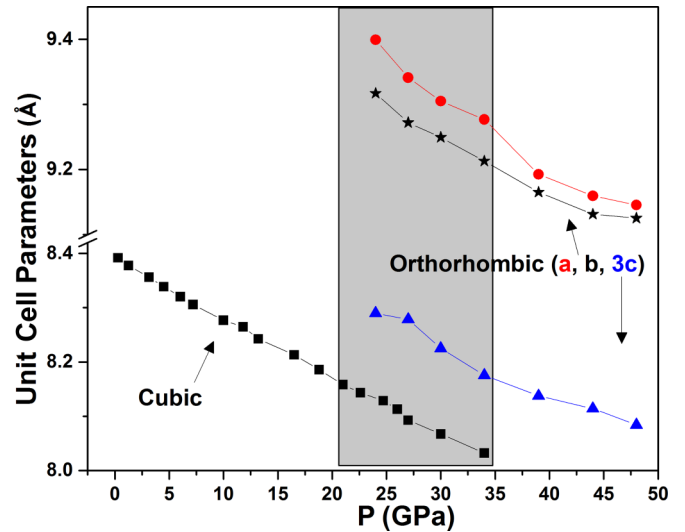


FIG. 3. Variation of unit cell parameters with  $P$  for spinel and postspinel phases.

$K'_0 = 3.6(4)$  for the HP phase, respectively. Both bulk moduli agree well within error bars. Our results indicate that these two phases have a similar compressibility. We noticed that the phase transition was partially reversible upon decompression, as shown in Fig. 2(b).

The variation of  $\text{Zn}_{0.2}\text{Mg}_{0.8}\text{Fe}_2\text{O}_4$  lattice parameters with  $P$  at RT was obtained from Rietveld refinements for all diffraction patterns, and the results are shown in Fig. 3. For the orthorhombic phase in its pressure range of stability, the change of lattice parameters  $a$ ,  $b$ , and  $c$  are 2.7%, 2.04%, and 2.41%, respectively. Therefore, the compression is slightly anisotropic.

## B. Pressure-dependent Raman spectroscopy

Raman spectra for  $\text{Zn}_{0.2}\text{Mg}_{0.8}\text{Fe}_2\text{O}_4$  were recorded as a function of  $P$  in the range of 100–850  $\text{cm}^{-1}$ , as shown in Fig. 4(a). At ambient pressure, six Raman modes were observed at 217, 333, 485, 647, 689, and 706  $\text{cm}^{-1}$  and assigned to the  $M_1$ ,  $M_2$ ,  $M_3$ ,  $M_4$ ,  $M_5$ , and  $M_6$  Raman modes, respectively. Theoretical analysis based on the factor-group approach predicted five Raman-active bands, namely,  $A_{1g}$ ,  $E_g$  (strong modes), and three  $T_{2g}$  (weak modes) [23]. Usually some extra modes associated with cation disorder are observed depending on the synthesis method [38,39]; however, this was not in our case. Our results agree well with previous Raman studies on similar spinels [17,18]. In our paper, we observed the following: (i) shifting of all the Raman modes to higher frequency with increasing pressures and the disappearance of the  $M_1$  mode at about 5.5 GPa, (ii) appearance of a new Raman mode at about 22 GPa, and (iii) complete disappearance (reduced intensity and merged with background) of all the Raman modes above 30 GPa.

The vanishing  $M_1$  modes at  $\sim 5.5$  GPa can be attributed to the discontinuous change in the Fe-O bond length, according to a previous study [40]. The Raman modes from 650–710  $\text{cm}^{-1}$  are related to  $A_{1g}$  symmetry and associated with the tetrahedral sublattices [41]. The spectrum recorded at ambient pressure

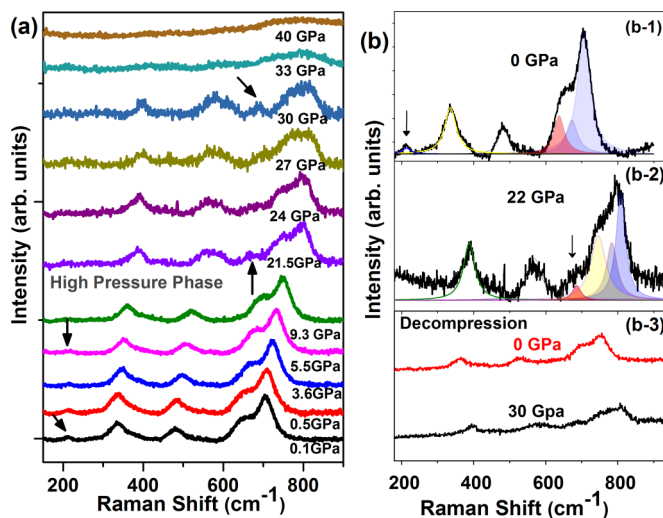


FIG. 4. (a) Raman spectra of  $\text{Zn}_{0.2}\text{Mg}_{0.8}\text{Fe}_2\text{O}_4$  at different pressures between 0 and 40 GPa, where Raman mode disappearance was observed at HP. (b) Deconvoluted spectra with Lorentzian fitting for Raman modes at (b-1) 0 GPa and at (b-2) 22 GPa. (b-3) Raman spectra for the same decompression cycle.

deconvoluted into three independent Lorentzian peaks, as shown in Fig. 4(b) (b-1), by taking the mass differences among the three ions ( $\text{Mg}^{2+}$ ,  $\text{Zn}^{2+}$ , and  $\text{Fe}^{3+}$ ) into account. The heaviest ( $\text{Zn}^{2+}$ ) and lightest ions ( $\text{Mg}^{2+}$ ) correspond to Raman modes 647 and 706  $\text{cm}^{-1}$ , respectively, and the 689  $\text{cm}^{-1}$  mode might correspond to the  $\text{Fe}^{3+}$  ion in the tetrahedral sublattice. At 22 GPa, near the cubic-orthorhombic phase transition, a new mode appeared at 667  $\text{cm}^{-1}$ , demonstrating the rearrangements of ions, as confirmed by earlier XRD measurements, and is shown in Fig. 4(b) (b-2). For  $P \geq 30$  GPa, all the Raman modes disappeared, which was likely due to either a structural transition or conductivity change. We will discuss this in a later section. In addition, we noticed that some of the Raman modes reappeared after the release of  $P$ , as shown in Fig. 4(b) (b-3), again indicating that the phase transition is partially reversible, in good agreement with our XRD results.

The pressure dependence of the Raman modes is plotted in Fig. 5, where significant changes of  $d\omega/dP$  are marked by a dashed line around 21 GPa. The analysis shows that every phonon mode increases linearly with  $P$  above and below the phase transition. With the bulk modulus calculated

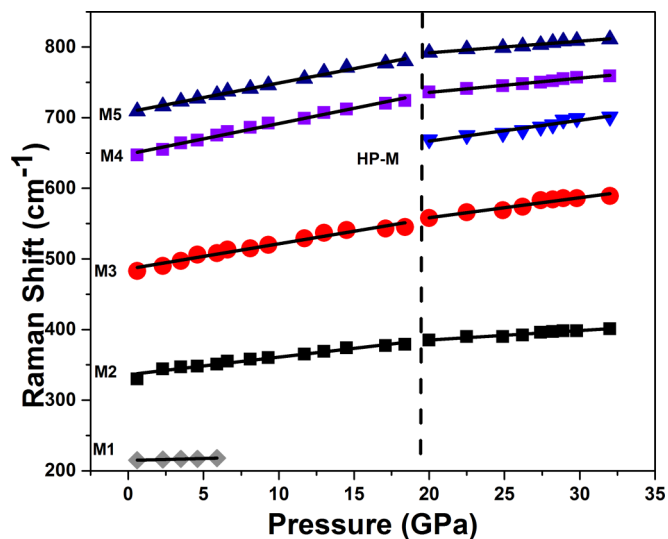


FIG. 5. Pressure dependence of the Raman modes at different pressures between 0 and 33 GPa, where solid lines show linear fits corresponding to specific modes.

from our XRD data and using the pressure derivative of a vibrational frequency, the Grüneisen parameters ( $\gamma$ ) were obtained using the equation  $\gamma = K_0/\omega_0(d\omega/dP)$ , where  $K_0$  is the bulk modulus and  $\omega_0$  is the frequency of the Raman shift observed at 1 atm. The coefficient value of the pressure shift,  $d\omega/dP$ , was obtained by fitting the relation between the frequency shift and pressure with a linear equation. The Grüneisen parameters  $\gamma$  of the cubic phase and HP phase are ranged in value from 0.48–1.45 and 0.37–0.97, respectively (Table I). The obtained mode Grüneisen parameters can be used to determine heat capacities and vibrational entropies using the Kieffer model [42,43]. The Grüneisen parameters of the Raman modes in the HP phase tend to be smaller than those in the ambient pressure phases. The comparison of the  $d\omega/dP$  obtained from our sample with pure  $\text{ZnFe}_2\text{O}_4$ ,  $\text{MgFe}_2\text{O}_4$  is consistent.

### C. Pressure-dependent electrical resistivity

Figure 6 shows the electrical resistivity  $\rho$  as a function of  $P$  at RT. In the cubic phase at RT,  $\rho$  is  $\sim 10^4 \Omega \text{ cm}$ , about three orders of magnitude smaller than  $\rho \sim 10^7 \Omega \text{ cm}$  of  $\text{MgFe}_2\text{O}_4$  because Zn partially replaces Mg in  $\text{MgFe}_2\text{O}_4$ . Partial substitution of octahedral Mg ions by tetrahedral Zn ions actually

TABLE I. Comparison of Raman modes, pressure coefficients  $d\omega/dP$ , and calculated Grüneisen parameters of  $\text{Zn}_{0.2}\text{Mg}_{0.8}\text{Fe}_2\text{O}_4$  polymorphs.

Low-pressure spinel phase			High-pressure orthorhombic phase		
Raman modes $\omega_0(\text{cm}^{-1})$	$d\omega/dP$ ( $\text{cm}^{-1}/\text{GPa}$ )	$\gamma$	Raman modes $\omega_0(\text{cm}^{-1})$	$d\omega/dP$ ( $\text{cm}^{-1}/\text{GPa}$ )	$\gamma$
217	0.54	0.48			
333	2.48	1.45	358	1.34	0.64
485	3.55	1.43	501	2.83	0.97
			608	2.9	0.82
647	4.3	1.3	695	2.01	0.49
706	4.1	1.13	759	1.65	0.37

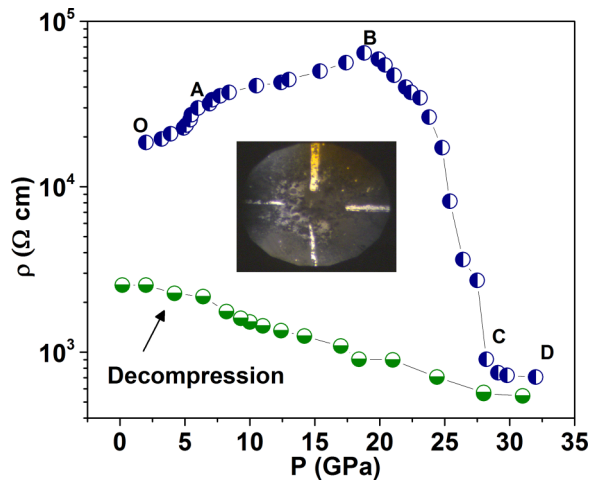


FIG. 6. Electrical resistance behavior of  $Zn_{0.2}Mg_{0.8}Fe_2O_4$  as a function of pressure at RT.

increases hopping conduction probability between  $Fe^{2+}$  and  $Fe^{3+}$  ions, and  $\rho$  decreases. Taking into account the RT mobility  $\mu \sim 1.6 \times 10^{-2} \text{ cm}^2/\text{V} - \text{s} [\frac{262}{T} \exp(-0.1/k_B T)]$  [44], we estimated the charge density as  $n_c \sim 10^{16}/\text{cm}^3$  and confirmed the spinel insulating character at ambient  $P$ . For  $P \leq 5$  GPa (region OA in the figure),  $\rho$  increases slowly. At higher pressure, it changes the slope of the pressure dependence (region AB). The subtle change in the pressure dependence of the resistivity can be correlated with the changes observed in the Raman spectra, while there are no changes shown in XRD. This indicates the occurrence of disordering in the local structure or a cation exchange induced by pressure. The disappearance of the  $M_1$  Raman mode related to changes in Fe-O bonds might be the reason for this change. From 5 to 19 GPa (region AB in Fig. 6),  $\rho$  increased almost linearly with slope  $d \ln(\rho)/dP \sim 0.051 \pm 0.006 \text{ GPa}^{-1}$  and reached its highest value of  $7 \times 10^4 \text{ } \Omega \text{ cm}$  at 19 GPa. The existence of the insulating cubic phase is compatible with the high  $\rho$ .

For  $P > 20$  GPa,  $\rho$  decreases sharply up to 27 GPa (region BC) and then becomes almost  $P$  independent with a value of  $8 \times 10^2 \text{ } \Omega \text{ cm}$  beyond 27 GPa (region CD). The change in resistivity is about two orders of magnitude. The rate of change of  $\rho$  in the BC region was  $\sim -0.434 \pm 0.021 \text{ GPa}^{-1}$ . Our XRD and Raman results showed that an orthorhombic phase started to develop at above 20 GPa, thus the emergence of this new phase explains the increase of electrical conductivity (decrease of resistivity) as pressure increases beyond 20 GPa. The 7 GPa region that covers the resistivity decrease is a consequence of the phase coexistence and gradual transformation of the sample from cubic to orthorhombic. Above 27 GPa, the change of resistance is negligible, and the charge density  $n_c$  was estimated to be about  $10^{18}/\text{cm}^3$ , two orders of magnitude larger than the ambient phase, by assuming  $\mu$  is constant over the whole region of  $P$  [45]. Nonetheless, the charge density of the observed HP phase is still four orders of magnitude lower than conventional metals. In the decompression cycle,  $\rho$  was partially recovered to  $\sim 1.5 \times 10^3 \text{ } \Omega \text{ cm}$  due to the failure of complete LP phase recovery from the mixture of HP and LP phases.

The postspinel orthorhombic  $CaTi_2O_4$  structure shows 18–24 Raman active modes [46], while none were identified during the metallization process at HP. Further investigations were performed by *in situ* optical microscopic imaging the sample during compression inside the DAC, as shown in Fig. 7. Figures 7(a)–7(d) correspond to the regions of OA, AB, BC, and CD in Fig. 6, respectively. The color changed from rust brown to black upon compression from ambient to 30 GPa, which clearly indicates a closure of the band gap.

To better understand our optical observations, we measured resistivity as a function of temperature at few fixed pressures, and the results are shown in Fig. 7(e). The slope of temperature dependent resistivity is negative,  $d\rho/dT < 0$  for  $P < 30$  GPa. The  $d\rho/dT$  is independent of temperature for pressures above 34 GPa, as shown in Fig. 7(e), which indicates metallization is expected to occur at lower pressure (30 GPa), as per our previous results (see Fig. 5). The sample appeared to be a bad

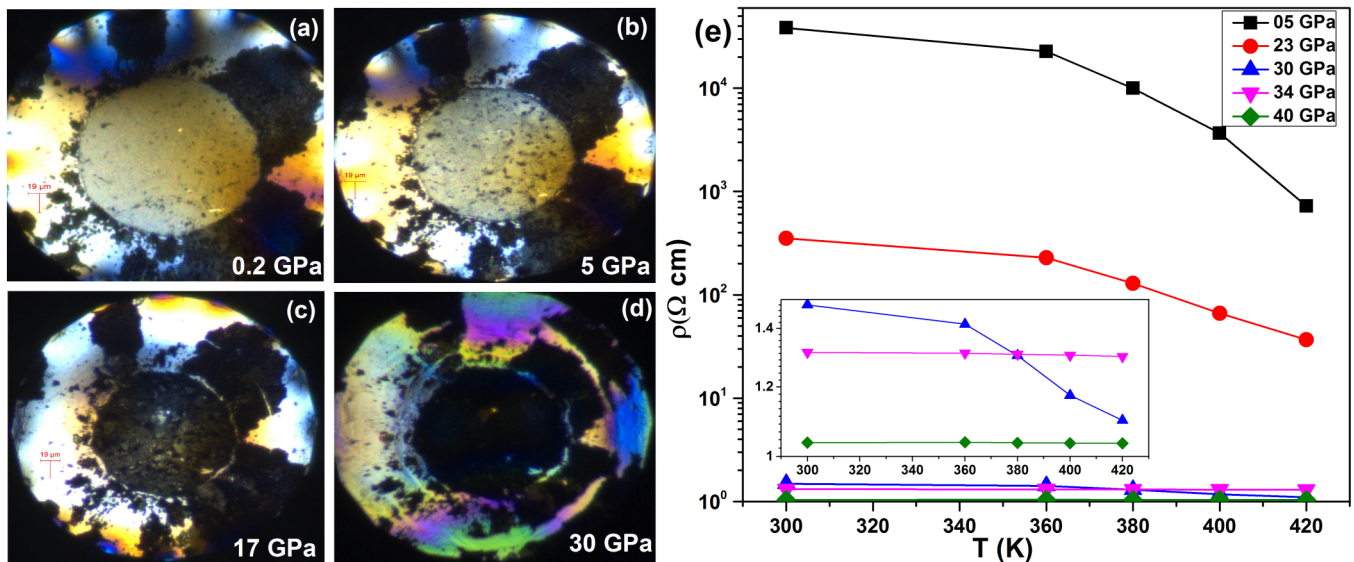


FIG. 7. (a)–(d) Color variations observed through low-resolution optical microscopic images captured in  $Zn_{0.2}Mg_{0.8}Fe_2O_4$  with increasing pressure. (e) Isobaric temperature-dependent resistivity for a few representative pressure values.

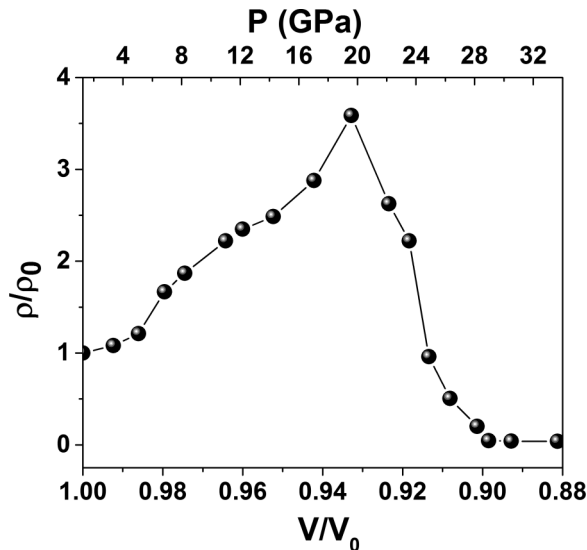


FIG. 8. Variation of normalized resistance with normalized volume fraction.

metal, in contrast to a conventional metal. Similar kinds of observations were noticed in past studies in strongly correlated materials, high- $T$  superconductors, and hydrides [47–50].

We plotted normalized resistivity  $\rho/\rho_0$  with normalized volume  $V/V_0$  in Fig. 8. A reduction in volume by around two orders of magnitude across the phase transition. In contrast, the change of resistivity below 20 GPa was much less pronounced. Hence, we conclude that the orthorhombic phase has a more dominant contribution to electrical conduction than the cubic phase. The pressure dependence of the resistivity shows there was no hint of band-gap ( $E_g$ ) closure for  $P < 20$  GPa. It is possible that at the LP region, Fe-O bonds are not decreased but increased with  $P$  and Fe-O-Fe bond angles change slightly with  $P$ . As a result, the formation of the conducting network receives hindrances at LP, thus  $\rho$  increases for  $P < 20$  GPa. This result differs from the resistivity scenario at the LP phase ( $\leq 10$  GPa) reported for  $\text{Fe}_3\text{O}_4$  [22], where reduction of  $\rho$  was explained by electron hopping between  $\text{Fe}^{2+}$  and  $\text{Fe}^{3+}$  ions by small polarons. In the HP region, a sharp drop of  $\rho$  shows band-gap closure manifests in an IMT beyond 20 GPa.

#### IV. DISCUSSION

Resistivity measurements, along with XRD and Raman spectroscopy, reveal a significant correlation between electronic and structural transitions in our mixed spinel ferrites above 20 GPa. According to the pressure dependence of resistivity above 20 GPa, a decrease of nearly two orders of magnitude within a 5 GPa range of pressure supports the onset of a metallic state above 25 GPa. Above 30 GPa, all the Raman modes vanish for our material, along with a drastic increase of reflectivity at HP, which is consistent with an IMT. In the same pressure range, a first-order phase transition with discontinuous volume change of 7.5% was observed.

In transition metal oxides, like our ferrites, insulating properties at ambient pressure and temperature can be attributed to a  $d-d$  energy gap (Mott-Hubbard gap) or a

$p-d$  gap, depending on which is their highest occupied band [51]. Mott insulators have magnetic states linked with the transition metal (here Fe) ion electronic state determined by Hund’s rule. Chemical doping or externally induced band broadening by pressure/temperature can rule the IMT. The pressure-induced breakdown of the  $d-d$  correlation with a collapse of magnetism suggests a band-width driven Mott IMT, as found in  $\text{GaFeO}_3$  [52]. Upon the IMT, the Fe-containing compounds have significant volume reduction of more than  $\sim 3\%$ , and in  $\text{Fe}_2\text{O}_3$  [53] it is as large as  $\sim 10\%$  at  $P \sim 50$  GPa, accompanied by a sharp IMT. The transition in  $\text{Fe}_2\text{O}_3$  corresponds to a Mott transition driven by a structural transition where band-gap closure is achieved by a change in the crystal structure.

The HP not only induces the change in crystal structure but also Mott-transition correlation breakdown with spin-crossover from a high-spin (HS) to low-spin (LS) transition, resulting in a pressure-induced increase of the crystal field. This phenomena leads to a substantial decrease of the magnetic moment for  $\text{Fe}^{3+}$  ( $S = 5/2 \rightarrow S = 1/2$ ) (ferric systems) and a complete collapse of the magnetic moment for  $\text{Fe}^{2+}$  ( $S = 2 \rightarrow S = 0$ ) (in ferrous systems) [54,55]. These phenomena are common in several orthoferrites, and all of them show reversible isostructural phase transitions driven by shrinkage of the  $\text{FeO}_6$  octahedra with large volume reduction at the transition. Merlini *et al.* [56] reported a decrease of molar volume change by 8.4% along with a 12% decrease in the Fe polyhedral volume, which is large in comparison with other  $\text{Fe}^{3+}$  oxides such as  $\text{GaFeO}_3$ . These transitions were also accompanied by a substantial decrease of electrical resistance, suggesting the spin crossover mechanism in the Fe sublattices resulted in band-gap closure with the IMT. Experimentally, in ferric compounds such as  $\text{CaFe}_2\text{O}_4$  [54], Mössbauer spectroscopy shows that the HS component completely vanishes where a new nonmagnetic phase appears upon compression. No trace of a magnetic hyperfine interaction for the  $\text{Fe}^{3+}$  LS state was found, which suggests a transition  $S = 5/2 \rightarrow S = 1/2$ . In  $\text{CaFe}_2\text{O}_4$ , Merlini *et al.* [56] concluded that such a HS-LS transition was caused by large volume reduction.

Undoped  $\text{ZnFe}_2\text{O}_4$  ( $[\text{Zn}_x^{2+}\text{Fe}_{1-x}^{3+}]_{\text{tet}}[\text{Fe}_{1-x}^{2+} + \text{Fe}_{1+x}^{3+}]_{\text{octa}}\text{O}_4^{2-}$ ) has octahedral-site (Fe) electronic configurations as a HS state ( $nd^5$ ) with no orbital degeneracy. Doping with Mg replaces  $\text{Fe}^{2+}$  at the octahedral sites and leaves the system with  $\text{Fe}^{3+}$  at both octahedral and tetrahedral sites, leaving our system as ferric compound [17,18]. Still, there must be some uncompensated  $\text{Fe}^{2+}$  ions in the systems, but their relative amount is difficult to estimate. For a composition of our sample,  $\text{Zn}_{0.2}\text{Mg}_{0.8}\text{Fe}_2\text{O}_4$ , more than 75% of the  $\text{Fe}^{3+}$ , is at octahedral sites [17,18]. Therefore, as a first approximation, the changes induced by pressure in the band gap can be associated to changes of the spin of  $\text{Fe}^{3+}$  at octahedral sites. By considering all the possibilities of the Mott transition, our experiments support a HS-LS transition amplified by structural consequences near the IMT. As Mössbauer spectroscopy does not show a LS state at the coexisting region of the LP and HP phases, it appears that the HS-LS transition leads to an IMT immediately [17,54,57,58]. The sharp nature of the IMT in  $\text{Zn}_{0.2}\text{Mg}_{0.8}\text{Fe}_2\text{O}_4$  supports this transition mechanism and also explains the huge volume change of 7.5% observed in our XRD experiments. We

suggest that, unlike  $\text{CaFe}_2\text{O}_4$ , our sample undergoes a pressure-induced IMT with a scenario similar to Hubbard-gap closure and different from a bandwidth controlled Mott transition.

Recent experimental and theoretical investigations [54,59–61] explained that the spin crossover phenomenon in transition metal ions is a result of the Hubbard band closure with simultaneous observations of volume collapse, magnetic moment collapse, and metallization. The large volume change of  $\sim 7.5\%$  observed in our system is a consequence of two processes, such as spin crossover and correlation breakdown. The electronic transition and the collapse of the insulating state to a metallic state, which results from the increasing crystal field splitting in mixed ferrites, has not been investigated to date. Our results are supported by the theoretical predictions made by Kunes *et al.* [60]. However, our conclusion should be further supported by complementary HP measurements of the  $\text{Fe}^{3+}$  spin state in  $\text{Zn}_{0.2}\text{Mg}_{0.8}\text{Fe}_2\text{O}_4$  by x-ray emission techniques. We hope the present results will trigger such studies.

## V. CONCLUSION

In summary, the structural, vibrational, and electronic properties of  $\text{Zn}_{0.2}\text{Mg}_{0.8}\text{Fe}_2\text{O}_4$  were explored by series of experimental techniques. A structural phase transition from a cubic to orthorhombic structure was observed. It occurred together with a Mott IMT at around 21 GPa. We also found that

above 30 GPa all Raman modes disappeared, which is consistent with the occurrence of metallization. The temperature-dependent resistivity showed nonmetallic behavior below 34 GPa and became independent with temperature above it, suggesting a bad-metallic behavior. The phase transition was associated with large crystal volume shrinkage, which was supported by the spin crossover mechanism of transition metal ions. The HP phase appeared as a bad metallic phase and decompression lead to partial recovery of the cubic phase at LP, as observed by XRD, Raman spectroscopy, and electrical resistivity measurements. Further experiments and theoretical studies on mixed spinel ferrites are necessary to completely characterize their pressure-induced metallization process.

## ACKNOWLEDGMENTS

Part of the paper was performed at the BL15U1 beamline, SSRF in China. We would like to acknowledge the support from Aiguo Li from SSRF. This paper was supported by National Science Associated Funding (Grant No. U1530402) and the “Science Challenging Program (Grant No. JCKY2016212A501)”. L.W. acknowledges the Program for New Century Excellent Talents in University (Program No. NCET-10-0444). S.R. also thanks the Anhui Government Scholarship. D.E. thanks the financial support of Spanish Ministerio de Economía, Industria y Competitividad de España (MINECO) under Grants No. MAT2016-75586-C4-1-P and No. MAT2015-71070-REDC (MALTA Consolider).

- 
- [1] D. Venkateshvaran, M. Althammer, A. Nielsen, S. Geprägs, M. S. Ramachandra Rao, S. T. B. Goennenwein, M. Opel, and R. Gross, *Phys. Rev. B* **79**, (2009).
- [2] A. Goldman, *Modern Ferrite Technology* (Van Nostrand, New York, 1990).
- [3] M. Kargarian, M. Randeria, and N. Trivedi, *Sci. Rep.* **5**, 12683 (2015).
- [4] E. Kojima, A. Miyata, S. Miyabe, S. Takeyama, H. Ueda, and Y. Ueda, *Phys. Rev. B* **77**, 212408 (2008).
- [5] W. Schiessl, W. Potzel, H. Karzel, M. Steiner, G. M. Kalvius, A. Martin, M. K. Krause, I. Halevy, J. Gal, W. Schäfer, G. Will, M. Hillberg, and R. Wäppling, *Phys. Rev. B* **53**, 9143 (1996).
- [6] K. P. Thummer, M. C. Chhantbar, K. B. Modi, G. J. Balधा, and H. H. Joshi, *J. Magn. Mater.* **280**, 23 (2004).
- [7] A. Pradeep, P. Priyadharsini, and G. Chandrasekaran, *J. Magn. Mater.* **320**, 2774 (2008).
- [8] Y. Ichiyonagi, M. Kubota, S. Moritake, Y. Kanazawa, T. Yamada, and T. Uehashi, *J. Magn. Mater.* **310**, 2378 (2007).
- [9] M. Francisco Javier, *Pressure-Induced Phase Transitions in AB<sub>2</sub>X<sub>4</sub> Chalcogenide Compounds* (Springer, Berlin, 2014).
- [10] B. S. Boyanov, *J. Thermal Anal.* **41**, 1607 (1994).
- [11] H. Suzuki, T. Furubayashi, G. Cao, H. Kitazawa, A. Kamimura, K. Hirata, and T. Matsumoto, *J. Phys. Soc. Jpn.* **68**, 2495 (1999).
- [12] S. Klemme and M. Ahrens, *Phys. Chem. Miner.* **32**, 374 (2005).
- [13] K. M. Rabe, *Annu. Rev. Condens. Matter Phys.* **1**, 211 (2010).
- [14] L. Zhang, Y. Meng, W. Yang, L. Wang, W. L. Mao, Q.-S. Zeng, J. S. Jeong, A. J. Wagner, K. A. Mkhoyan, W. Liu, R. Xu, and H.-k. Mao, *Science* **344**, 877 (2014).
- [15] S. Ferrari, R. S. Kumar, F. Grinblat, J. C. Apesteguy, F. D. Saccone, and D. Errandonea, *Solid State Sci.* **56**, 68 (2016).
- [16] D. Andrault and N. Bolfan-Casanova, *Phys. Chem. Miner.* **28**, 211 (2001).
- [17] S. W. da Silva, F. Nakagomi, M. S. Silva, A. Franco, Jr., V. K. Garg, A. C. Oliveira, and P. C. Morais, *J. Nanopart. Res.* **14**, 1 (2012).
- [18] S. W. da Silva, F. Nakagomi, M. S. Silva, A. Franco, V. K. Garg, A. C. Oliveira, and P. C. Morais, *J. Appl. Phys.* **107**, 09B503 (2010).
- [19] S. Rahman, K. Nadeem, M. Anis-ur-Rehman, M. Mumtaz, S. Naeem, and I. Letofsky-Papst, *Ceram. Int.* **39**, 5235 (2013).
- [20] Y. Fei, D. J. Frost, H.-K. Mao, C. T. Prewitt, and D. Haeusermann, *Am. Mineral.* **84**, 203 (1999).
- [21] C. Haavik, *Am. Mineral.* **85**, 514 (2000).
- [22] E. R. Morris and Q. Williams, *J. Geophys. Res. Solid Earth* **102**, 18139 (1997).
- [23] G. Gusmano, G. Montesperelli, P. Nunziante, and E. Traversa, *J. Mater. Sci.* **28**, 6195 (1993).
- [24] C. Doroftei, E. Rezlescu, N. Rezlescu, and P. D. Popa, *Rom. J. Phys.* **51**, 631 (2006).
- [25] M. Javed Iqbal, Z. Ahmad, T. Meydan, and Y. Melikhov, *J. Appl. Phys.* **111**, 033906 (2012).
- [26] B. Gillot, R. M. Benloucif, and A. Rousset, *Phys. Status Solidi A* **65**, 205 (1981).
- [27] H. K. Mao, D. Virgo, and P. M. Bell, *Carnegie Inst. Wash. Yearb.* **76**, 522 (1977).
- [28] M. P. Pasternak, S. Nasu, K. Wada, and S. Endo, *Phys. Rev. B* **50**, 6446 (1994).
- [29] D. Levy, A. Pavese, and M. Hanfland, *Phys. Chem. Miner.* **27**, 638 (2000).

- [30] Z. Wang, P. Lazor, S. K. Saxena, and H. S. C. O'Neill, *Mater. Res. Bull.* **37**, 1589 (2002).
- [31] B. Xiao, W. Zheng, M. Zhu, W. Zhao, N. Ma, and P. Du, *J. Mater. Chem. C* **2**, 7482 (2014).
- [32] H. Mao, J.-A. Xu, and P. Bell, *J. Geophys. Res. Solid Earth* **91**, 4673 (1986).
- [33] J. Rodríguez-Carvajal, *Physica B* **192**, 55 (1993).
- [34] D. Errandonea, A. Segura, D. Martínez-García, and V. Muñoz-San Jose, *Phys. Rev. B* **79**, 125203 (2009).
- [35] E. Greenberg, G. K. Rozenberg, W. Xu, R. Arielly, M. P. Pasternak, A. Melchior, G. Garbarino, and L. S. Dubrovinsky, *High Press. Res* **29**, 764 (2009).
- [36] Z. Wang, R. T. Downs, V. Pischedda, R. Shetty, S. K. Saxena, C. S. Zha, Y. S. Zhao, D. Schiferl, and A. Waskowska, *Phys. Rev. B* **68**, 094101 (2003).
- [37] S. Ono, T. Kikegawa, and Y. Ohishi, *Phys. Chem. Miner.* **33**, 200 (2006).
- [38] P. R. Graves, C. Johnston, and J. J. Campaniello, *Mater. Res. Bull.* **23**, 1651 (1988).
- [39] W. B. White and B. A. DeAngelis, *Spectrochim. Acta Mol. Spectrosc.* **23**, 985 (1967).
- [40] H. Kobayashi, I. Isogai, T. Kamimura, N. Hamada, H. Onodera, S. Todo, and N. Mōri, *Phys. Rev. B* **73**, 104110 (2006).
- [41] J. Kreisel, G. Lucazeau, and H. Vincent, *J. Solid State Chem.* **137**, 127 (1998).
- [42] S. W. Kieffer, *Rev. Geophys.* **17**, 1 (1979).
- [43] S. W. Kieffer, *Rev. Geophys.* **17**, 20 (1979).
- [44] R. F. G. Gardner, R. L. Moss, and D. W. Tanner, *Br. J. Appl. Phys.* **17**, 55 (1966).
- [45] D. Errandonea, E. Bandiello, A. Segura, J. J. Hamlin, M. B. Maple, P. Rodríguez-Hernandez, and A. Muñoz, *J. Alloys Compd.* **587**, 14 (2014).
- [46] S. López-Moreno, P. Rodríguez-Hernández, A. Muñoz, A. H. Romero, F. J. Manjón, D. Errandonea, E. Rusu, and V. V. Ursaki, *Ann. Phys. (Berlin)* **523**, 157 (2011).
- [47] H. Nguyen, Z. Chi, T. Matsuoka, T. Kagayama, and K. Shimizu, *J. Phys. Soc. Jpn.* **81**, SB041 (2012).
- [48] M. M. Qazilbash, K. S. Burch, D. Whisler, D. Shrekenhamer, B. G. Chae, H. T. Kim, and D. N. Basov, *Phys. Rev. B* **74**, 205118 (2006).
- [49] O. Gunnarsson, M. Calandra, and J. E. Han, *Rev. Mod. Phys.* **75**, 1085 (2003).
- [50] S. Samanta, A. K. Raychaudhuri, X. Zhong, and A. Gupta, *Phys. Rev. B* **92**, 195125 (2015).
- [51] J. Zaanen, G. A. Sawatzky, and J. W. Allen, *Phys. Rev. Lett.* **55**, 418 (1985).
- [52] R. Arielly, W. M. Xu, E. Greenberg, G. K. Rozenberg, M. P. Pasternak, G. Garbarino, S. Clark, and R. Jeanloz, *Phys. Rev. B* **84**, 094109 (2011).
- [53] G. K. Rozenberg, L. S. Dubrovinsky, M. P. Pasternak, O. Naaman, T. Le Bihan, and R. Ahuja, *Phys. Rev. B* **65**, 064112 (2002).
- [54] E. Greenberg, G. K. Rozenberg, W. Xu, M. P. Pasternak, C. McCammon, K. Glazyrin, and L. S. Dubrovinsky, *Phys. Rev. B* **88**, 214109 (2013).
- [55] S. Speziale, A. Milner, V. E. Lee, S. M. Clark, M. P. Pasternak, and R. Jeanloz, *Proc. Natl. Acad. Sci. U.S.A.* **102**, 17918 (2005).
- [56] M. Merlini, M. Hanfland, M. Gemmi, S. Huotari, L. Simonelli, and P. Strobel, *Am. Mineral.* **95**, 200 (2010).
- [57] J. Badro, G. Fiquet, V. V. Struzhkin, M. Somayazulu, H.-k. Mao, G. Shen, and T. Le Bihan, *Phys. Rev. Lett.* **89**, 205504 (2002).
- [58] G. K. Rozenberg, W. Xu, and M. P. Pasternak, *Z. Kristallogr. Cryst. Mater.* **229**, 210 (2014).
- [59] W. M. Xu, O. Naaman, G. K. Rozenberg, M. P. Pasternak, and R. D. Taylor, *Phys. Rev. B* **64**, 094411 (2001).
- [60] J. Kunes, A. V. Lukoyanov, V. I. Anisimov, R. T. Scalettar, and W. E. Pickett, *Nat. Mater.* **7**, 198 (2008).
- [61] A. G. Gavriluk, V. V. Struzhkin, I. S. Lyubutin, S. G. Ovchinnikov, M. Y. Hu, and P. Chow, *Phys. Rev. B* **77**, 155112 (2008).